

Fast and Accurate Neural Rendering Using Semi-Gradients

IN-YOUNG CHO and JAEWOONG CHO, KRAFTON, Republic of Korea



Fig. 1. Rendering residual-based optimization results of the baseline, based on Neural Radiosity [Hadadan et al. 2021], and the proposed method for neural rendering. Previous approaches minimize the L2 distance between the left-hand side (i.e., outgoing radiance) and the right-hand side (i.e., the sum of emitted and reflected radiance) of the rendering equation. We discover that the bias and high variance of the baseline gradient estimator lead to poor convergence, and we propose a partial derivative-based optimization method to resolve them. The graph on the right shows the change in image-space distance from the reference as training progresses.

We propose a simple yet effective neural network-based framework for global illumination rendering. Recently, rendering techniques that learn neural radiance caches by minimizing the difference (i.e., residual) between the left and right sides of the rendering equation have been suggested. Due to their ease of implementation and the advantage of excluding path integral calculations, these techniques have been applied to various fields, such as free-viewpoint rendering, differentiable rendering, and real-time rendering. However, issues of slow training and occasionally darkened renders have been noted. We identify the cause of these issues as the bias and high variance present in the gradient estimates of the existing residual-based objective function. To address this, we introduce a new objective function that maintains the same global optimum as before but allows for unbiased and low-variance gradient estimates, enabling faster and more accurate training of neural networks. In conclusion, this method is simply implemented by ignoring the partial derivatives of the right-hand side, and theoretical and experimental analyses demonstrate the effectiveness of the proposed loss.

CCS Concepts: • **Computing methodologies** → **Ray tracing; Neural networks**.

Additional Key Words and Phrases: Neural Rendering, Neural Radiance Fields, Global Illumination, Gradient-based Optimization

1 INTRODUCTION

Neural network-based methods have recently received remarkable attention in global illumination rendering domain. This is primarily due to the scalability and high fidelity of neural networks, which help alleviate the computational burden and noise associated with traditional Monte Carlo (MC) methods. Among these methods, some apply neural networks to the precomputation or caching processes that have long been common in rendering.

In particular, Hadadan et al. [2021]; Müller et al. [2021] replace the outgoing radiance field on both the left-hand side (LHS) and right-hand side (RHS)—the sum of the emitted and reflected radiance—of the rendering equation with a neural network. They introduce

objective functions that minimize the L2 distance between the two. These approaches use a neural network to approximate the RHS, employing fewer ray tracing iterations instead of extensive path tracing. This not only makes the approach appealing for reducing memory incoherent operations during rendering but also during the learning phase of neural caches.

While there have been various applications of this technique to real-time rendering or differentiable rendering [Coomans et al. 2024; Hadadan et al. 2023], substantial dialogue regarding methods to accelerate the training of neural networks remains scarce. Meanwhile, we observe that during training using rendering residuals, the RHS converges much faster than the LHS (Fig. 2). Consequently, we hypothesize that the existing loss, which optimizes the LHS and RHS to get closer to each other, might hinder convergence. This happens because the RHS, which is already close to the reference, is updated towards the LHS, which is still far from the reference.

Therefore, we theoretically derive that using only the partial derivatives for the LHS can still lead neural caches to converge to the solution of the rendering equation, and we define this as the *semi-gradient* method. Our results, also exemplified in Fig. 1, show that in comparisons of identical training iterations with the baseline [Hadadan et al. 2021], the error to the reference decreases by an average of 8.8 times across various scenes, and training time is reduced by 25-30%.

Through theoretical and experimental analysis, we demonstrate that the stochasticity of MC integration (e.g., RHS) and its noisy derivatives cause gradient bias and high variance. This issue has also been pointed out in the differentiable rendering domain [Azinovic et al. 2019; Nimier-David et al. 2020]. In contrast, our proposed method effectively mitigates this error in forward rendering by removing the partial derivatives for the RHS, the main source of the error.

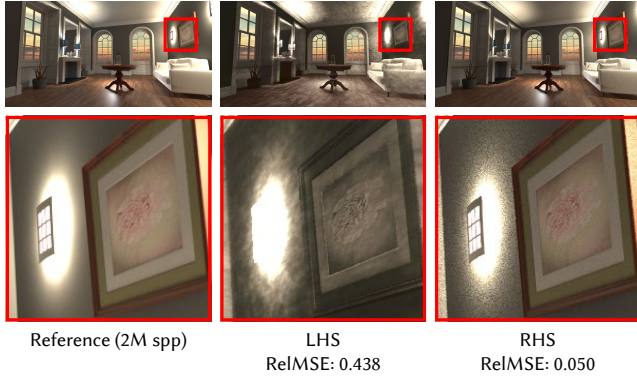


Fig. 2. Example to motivate our partial derivative-based optimization for faster convergence. From the start of training (100 iterations, 14 seconds) of the baseline (Sec. 3.1), the RHS quickly converges to the reference, while the LHS lags behind with issues such as faint colors and brightness overshoot on lampshades. As such, we ignore the partial derivative with respect to the RHS, focusing on learning the LHS. For visualization, the LHS and the RHS are shown at 4 and 1024 samples-per-pixel (spp), respectively.

2 RELATED WORK

2.1 Neural Caches for Global Illumination

Recently, deep learning-based caching techniques for rendering have been applied in various ways. Some methods employ supervised learning techniques, training neural networks using pre-collected reference renders and then utilizing the networks to render other scenes. Rainer et al. [2022]; Zhu et al. [2021] use neural caches to learn objects illuminated by environment maps and complex luminaires, respectively. Dong et al. [2023]; Huang et al. [2024] design neural networks that decode parametric mixtures for path guiding.

Meanwhile, *self-training* methods, which train neural caches to restore radiance fields without using ground-truth renders, are also actively discussed. To achieve this, Hadadan et al. [2021]; Müller et al. [2021] use the rendering equation as a strong constraint that the radiance field must satisfy, in free-viewpoint rendering and real-time rendering, respectively. Since the outgoing radiance field (at equilibrium) always represents the sum of emitted and reflected radiance, the neural cache is trained to minimize the residual of the rendering equation. This discussion has been extended to real-time dynamic scene rendering and inverse rendering by Coomans et al. [2024]; Hadadan et al. [2023] respectively.

We focus on improving the convergence of this intriguing technique that allows learning caches without target radiance. Specifically, Hadadan et al. [2021, 2023] use the gradient for the RHS in optimization, while Coomans et al. [2024]; Müller et al. [2021] deactivate it. However, clear discussions supporting these choices have been scarce. Additionally, the reference implementation of Hadadan et al. [2021] acknowledges the idea of deactivation, but the paper does not study this choice. Therefore, we revisit the losses and support the semi-gradient method through experimental and theoretical analysis (Sec. 5).

2.2 Gradient Estimation for Learning and Rendering

Gradient estimation is crucial for optimization techniques that rely on stochastic gradient descent (SGD), such as neural caching, differentiable rendering, and deep learning.

Differentiable rendering also aims to estimate accurate image gradients to optimize scene parameters. Azinovic et al. [2019]; Nimier-David et al. [2020] highlight that gradient estimates can be biased when optimizing with MC samples, potentially distorting the converged scene parameters. To address this, methods such as using two uncorrelated samples for the rendering integral and its derivatives [Azinovic et al. 2019; Nimier-David et al. 2020; Vicini et al. 2021], employing dual-buffer techniques for the L2 loss [Deng et al. 2022; Pidhorskyi et al. 2022], and exploiting variance reduction techniques [Balint et al. 2023; Fischer and Ritschel 2023; Nicolet et al. 2023; Wang et al. 2023; Zhang et al. 2021] have been proposed.

Reinforcement learning (RL) learns optimal actions by minimizing the residual of the Bellman integral equation [Baird 1995]. However, in real-world scenarios, using uncorrelated samples is not always possible. Thus, empirical methods that utilize only the semi-gradient of the Bellman equation are employed [Mnih et al. 2015]. Despite the wide adoption of the semi-gradient method, a clear theoretical analysis of its convergence and effectiveness remains open [Sharifnassab and Sutton 2023; Yin et al. 2022; Zhang et al. 2019].

We show that gradient estimates for the rendering residual are also biased due to MC samples. Intriguingly, while the dual-buffer method effectively addresses this bias, the convergence of neural caches still remains slow. We found that this is due to the high variance of the RHS partial derivatives, which requires spending 16 times more time to extract 8 times more samples to resolve the issue (Sec. 5). However, we demonstrate that completely removing the RHS partial derivatives (*semi-gradient*) is more effective for convergence.

3 NEURAL RENDERING USING SEMI-GRADIENTS

3.1 Preliminaries and Baseline Method

The rendering equation [Kajiya 1986] serves as the cornerstone of physically-based rendering, representing the spatio-directional radiance field at equilibrium L^* :

$$L^*(x, \omega) = E(x, \omega) + \int_{\Omega} L^*(r(x, \omega_{\text{in}}), -\omega_{\text{in}}) f_s(x, \omega, \omega_{\text{in}}) |n^T \omega_{\text{in}}| d\omega_{\text{in}}. \quad (1)$$

In short, the equation states that the radiance L^* outgoing from a point x in a direction ω is always due to two sources: 1) emission $E(x, \omega)$ at the surface (e.g., in the case of a light source), and 2) reception from the surroundings. $f_s(x, \omega, \omega_{\text{in}})$ is the bidirectional scattering distribution function (BSDF), $|n^T \omega_{\text{in}}| d\omega_{\text{in}}$ is the differential of the projected solid angle between a surface normal n and an incident direction ω_{in} , and r is the ray tracing operation.

To train neural radiance caches that satisfy the rendering equation, Coomans et al. [2024]; Hadadan et al. [2021, 2023]; Müller et al. [2022] sample (x, ω) on meshes and a unit hemisphere in each training iteration. They approximate the LHS and RHS using neural networks and train the network by minimizing the L2 norm of the

residuals. The loss is formulated as follows:

$$\mathcal{L}(\theta) = \frac{\|L_\theta - R_\theta\|^2}{\|\text{sg}(L_\theta)\|^2 + \epsilon}. \quad (2)$$

Here, L_θ is a neural network parameterized by θ that approximates L^* , and R_θ represents the RHS of the rendering equation with L_θ substituted for L^* in the integrand. For brevity, the (x, ω) notation is omitted. The $\text{sg}(\cdot)$ denotes the stop-gradient operation, which ignores the gradient during the backward pass of automatic differentiation:

$$\begin{aligned} \text{sg}(x) &= x, \\ \nabla_x \text{sg}(x) &= 0. \end{aligned} \quad (3)$$

Note that this is a notation for implementation convenience, not a mathematically rigorous operation.

To approximate the above loss over the entire mesh and hemisphere space, Hadadan et al. [2021] uniformly sample (x, ω) . For each (x, ω) , the MC estimate for R_θ is calculated as follows to compute $\mathcal{L}(x, \omega; \theta)$:

$$\langle R_\theta \rangle = E + \frac{1}{M} \sum_{j=1}^M \frac{L_\theta(r(\omega_{\text{in},j}), -\omega_{\text{in},j}) f_s(\omega_{\text{in},j}) |n^\top \omega_{\text{in},j}|}{p(\omega_{\text{in},j})}, \quad (4)$$

where $\langle \cdot \rangle$ denotes an estimator (whether it is biased or not), M is the incident sample count and $p(\omega_{\text{in}}|x, \omega)$ is the probability density function (PDF) from which an incident direction is sampled. As long as the support of the PDF includes the support of the numerator, this MC estimate is an unbiased estimate of R_θ .

Finally, the original loss is approximated through the aforementioned sampling as follows:

$$\langle \mathcal{L}(\theta) \rangle_{\text{NR}} = \frac{\|L_\theta - \langle R_\theta \rangle\|^2}{\|\text{sg}(L_\theta)\|^2 + \epsilon}. \quad (5)$$

Here, NR stands for Neural Radiosity, the pioneering work by Hadadan et al. [2021]. The gradient estimator for optimizing this loss is approximated as follows:

$$\begin{aligned} \nabla_\theta \langle \mathcal{L}(\theta) \rangle_{\text{NR}} &= \nabla_\theta L_\theta \cdot \partial_{L_\theta} \langle \mathcal{L}(\theta) \rangle_{\text{NR}} + \nabla_\theta \langle R_\theta \rangle \cdot \partial_{\langle R_\theta \rangle} \langle \mathcal{L}(\theta) \rangle_{\text{NR}} \\ &= \nabla_\theta L_\theta \cdot \frac{2(L_\theta - \langle R_\theta \rangle)}{\|L_\theta\|^2 + \epsilon} + \nabla_\theta \langle R_\theta \rangle \cdot \frac{-2(L_\theta - \langle R_\theta \rangle)}{\|L_\theta\|^2 + \epsilon}. \end{aligned} \quad (6)$$

We note that $\text{sg}(\cdot)$ disappears in gradient evaluation. In Sec. 5, we show that this gradient estimator is a *biased* estimator of the gradient of Eq. (2). We reveal that it, along with high variance, hinders convergence. The common training procedure is summarized in Algorithm 1 with the **red background**.

3.2 Semi-Gradient Method

We previously raised the question in Sec. 1 and Fig. 2 whether it is necessary to update R_θ towards L_θ . Indeed, the RHS partial derivative in Eq. (6) can be seen as instructing the network to pull the RHS estimates towards the LHS. To prevent this, we replace the loss in the baseline training procedure with the following:

$$\langle \mathcal{L}(\theta) \rangle_{\text{SG}} = \frac{\|L_\theta - \text{sg}(\langle R_\theta \rangle)\|^2}{\|\text{sg}(L_\theta)\|^2 + \epsilon}. \quad (7)$$

Thanks to the stop-gradient operation introduced in the numerator, $\partial_{\langle R_\theta \rangle} \langle \mathcal{L}(\theta) \rangle_{\text{SG}} = 0$, achieving our intended goal. Here, SG stands

Algorithm 1 Color-coding the changes of our method compared to the baseline

Require: Initialize network parameters θ and the learning rate η

- 1: **while** not converged **do**
- 2: Sample location vectors $\{x_j\}_{j=1}^N$ uniformly on meshes
- 3: Sample the outgoing directions $\{\omega_j\}_{j=1}^N$ uniformly over a hemisphere
- 4: **for** each (x_j, ω_j) **do**
- 5: Sample incident directions $\{\omega_{\text{in},j,k} | k = 1, \dots, M\}$ uniformly over a hemisphere
- 6: **end for**
- 7: - Evaluate $\langle \mathcal{L}(\theta) \rangle_{\text{NR}}$ via the above samples
- 8: + Evaluate $\langle \mathcal{L}(\theta) \rangle_{\text{SG}}$ via the above samples
- 9: - $\theta \leftarrow \theta - \eta \cdot \nabla_\theta \langle \mathcal{L}(\theta) \rangle_{\text{NR}}$
- 10: + $\theta \leftarrow \theta - \eta \cdot \nabla_\theta \langle \mathcal{L}(\theta) \rangle_{\text{SG}}$
- 11: **end while**
- 12: **return** θ

for the *semi-gradient* method, as opposed to the full-gradient method. Therefore, the gradient estimator for optimizing this loss is evaluated as follows:

$$\nabla_\theta \langle \mathcal{L}(\theta) \rangle_{\text{SG}} = \nabla_\theta L_\theta \cdot \frac{2(L_\theta - \langle R_\theta \rangle)}{\|L_\theta\|^2 + \epsilon}. \quad (8)$$

However, for radiance caching, it must be ensured that the neural cache updated along this new gradient converges to the solution of the rendering equation. In Appendix A, we theoretically derive that convergence can be guaranteed for scenes satisfying the energy absorption condition [Neumann and Neumann 1995]. It is important to note that due to the mathematical shortcomings in the definition of the stop-gradient operation, the convergence of this L2-form loss cannot be prematurely guaranteed. For formalism regarding the expression and evaluation of the stop-gradient operation, refer to Ścibior and Wood [2021].

Additionally, although semi-gradient formulations have been utilized in reinforcement learning through temporal difference methods, as well as in neural rendering [Coomans et al. 2024; Müller et al. 2022], a distinct theoretical explanation of the effectiveness has not been thoroughly explored. We provide both theoretical and experimental analyses from a light transportation perspective.

Finally, Sec. 4 empirically shows that this subtle yet crucial alteration significantly enhances performance. Sec. 5 provides theoretical and experimental explanations for the improvement. Algorithm 1 summarizes the overall training procedure with the **green background**.

3.3 Implementation

We implement the baseline algorithm and our models following the PyTorch-based implementation by Cho [2023]. All radiance prediction networks consist of seven linear layers of 512 units with six ReLU activations; the last output of the linear layer does not go through an activation layer.

Network parameters are initialized using the Xavier uniform distribution [Glorot and Bengio 2010]. As previously noted, the training employs the Adam optimizer [Kingma and Ba 2014] with a learning rate set to 5×10^{-4} . The batch size for (x, ω) (i.e., N in the

Algorithm 1) is set to 2^{14} at the beginning, and for each (x, ω) , 32 incident directions are sampled (i.e., M). A radiance field network is trained for 36,000 steps separately for each scene. The learning rate is reduced by a third every 12,000 steps. We utilize the emission reparameterization trick proposed in the original work [Hadadan et al. 2021] to ensure stable training.

Training is performed on a single NVIDIA A100 GPU, with models using 7GB or less of VRAM. Training times vary depending on scene complexity and models, ranging from 40 minutes to 3.5 hours.

We use Mitsuba 3 [Jakob et al. 2022], which integrates smoothly with PyTorch for all rendering tasks in Algorithm 1. As suggested by Dong et al. [2023]; Hadadan et al. [2021], neural networks are fed with not only position and direction vectors but also texture, normal, and multi-resolution encoding inputs.

Variance reduced gradient estimator. To expedite initial convergence, we integrate the neural path guiding technique [Dong et al. 2023] into our framework. Additional neural caches are employed for sampling incident directions, comprising four linear layers of 256 units with three activations. These tiny caches result in negligible overhead compared to the baseline BSDF sampling. During 1,000 to 5,000 iterations, this module is trained alongside radiance caches, while held fixed for the remaining iterations.

This path guiding model operates with next event estimation for multiple importance sampling, aiding in the reduction of the variance of the RHS estimates and subsequently decreasing the variance of the semi-gradient estimator (Eq. (8)). This reduction is often instrumental in mitigating visual artifacts during early training stages and accelerating error reduction [Liu et al. 2020; Wang et al. 2013]. However, the variance-reduced gradient does not impact the error at final convergence, the primary focus of our discussion. Please refer to Fig. 10 in the Appendix for the ablation study on variance reduction.

3.4 Speedup Tricks Across Comparative Models

Neural Radiosity is an innovative method, but it often requires significant training time compared to state-of-the-art MC methods. We apply common modifications to all models to fasten training and rendering, resulting in approximately 2-fold faster processing. Specifically, we use the tiny-cuda-nn library [Müller 2021] to implement all networks. We also replace the multi-resolution feature grid with hash encoding from InstantNGP [Müller et al. 2022], which is also employed by Dong et al. [2023]. For the multi-resolution hash encoding, we set the base resolution to 2, the number of hierarchy levels to 14, the number of features per level to 2, and the hashmap size to 18 (in log scale).

Additionally, both training and rendering use mixed precision, which does not noticeably affect the quality of results. Thus, inputs like (x, ω) are rendered in 32-bit full precision and then converted to 16-bit half-precision when fed into the network. The network outputs are converted back to full precision before being ingested by the rendering engine.

Last but not least, to fully realize the speedup of the semi-gradient technique, we emphasize that unnecessary intermediate activations should not be stored for the backward pass, for example, by using the *no-grad* context manager in PyTorch [Paszke et al. 2017].

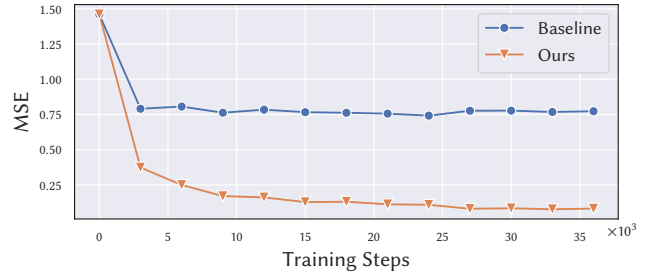


Fig. 3. Equal-iteration comparisons for our method and the baseline approach. The figure displays the convergence of image error, averaged across seven scenes in Fig. 9. Our method shows an average error that is 8.8 times lower.

Table 1. Comparison of time taken per iteration during training between the baseline and our method (in seconds). Our method takes 25-30% less time.

	Baseline	Ours
Bed	0.207	0.138
Bidir	0.096	0.066
Bath	0.208	0.143
Door	0.099	0.071
Greyroom	0.170	0.128
Hall	0.113	0.078
TVRoom	0.342	0.240

4 RESULTS

4.1 Dataset and Evaluation

We evaluate the performance of all models mainly across seven scenes with diverse interactions between materials and lights. To assess the convergence process, rendering via radiance prediction network is performed on a view determined for each scene every 3,000 steps and compared with the reference image. Metrics such as MSE, MAPE, and ReLMSE are measured at high-definition resolutions of either 960×960 or $1,280 \times 720$.

The reference images were rendered using 256K samples-per-pixel (spp), and the reference videos were rendered using 4K spp for each frame, followed by post-processing with OptiX denoiser [Parker et al. 2010] introduced in Mitsuba 3. Rendering every frame of a video with 256K spp would be too costly, so we used fewer spp and then applied denoising as post-processing for the reference videos. This approach more closely resembles the typical rendering process. All neural renderings, except RHS renderings, utilized four spp.

4.2 Training Efficiency Comparison

Fig. 10 demonstrates that the proposed method significantly enhances per-iteration convergence compared to the baseline. Our method achieves final errors with the reference images that are nine times lower than those of the baseline loss approach on average.

Our method reduces the per-iteration cost as well. Table 1 shows that ours reliably reduces the time to train models by 25-30% across all benchmarks. This efficiency is primarily due to the elimination

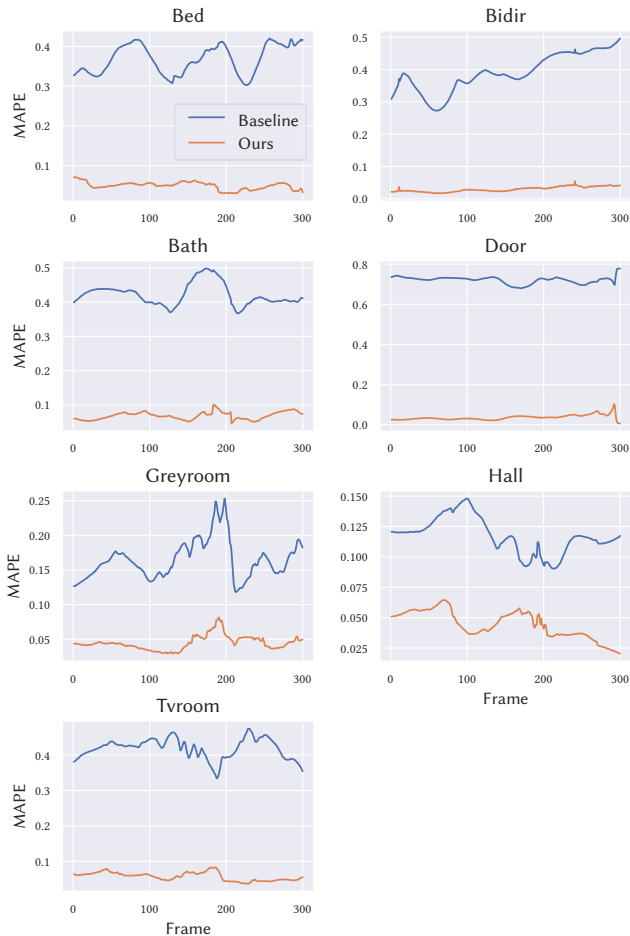


Fig. 4. When rendering free-viewpoint video along a camera path in each scene after training, the error of our method is lower than the baseline in all frames. Refer to the supplementary materials for the videos.

of partial derivatives for the RHS, which obviates the need to store intermediate activations in memory.

4.3 Rendering Fidelity Comparison

Fig. 9 demonstrates that, once all models have fully converged after 36,000 training steps, our model renders images of higher quality both numerically and visually compared to the baseline. The baseline tends to underestimate the energy irradiated in a scene and fails to capture bright highlights, color bleeding, or other indirect illumination features. Our framework addresses these limitations.

Lastly, Fig. 4 shows that our performance is not just confined to a specific view in each scene. Consistent benefits of the proposed framework are observed in every frame of videos, rendered along camera paths traversing each scene. We observe a significant reduction in MAPE, with errors decreasing by a factor of 2 to 35 times compared to the baseline. The supplementary materials include videos for reference.

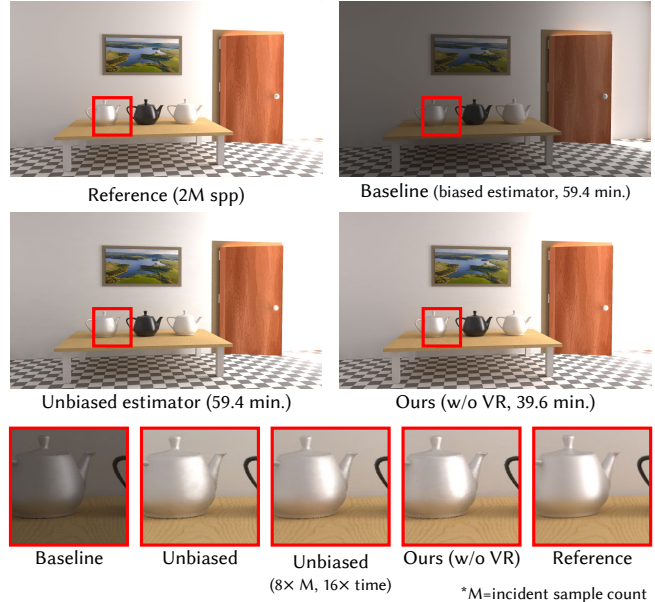


Fig. 5. Visual comparison between the baseline (biased gradient estimator), dual-buffer (unbiased gradient estimator) [Deng et al. 2022; Pidhorskyi et al. 2022], and our methods. When using the baseline method, the resulting reconstruction is noticeably darker. The dual-buffer approach resolves the bias on gradients yet fails to reconstruct glossy reflections shapely in the same training iterations. Increasing the incident sample count eightfold (to 256), taking 16-fold time, is necessary to achieve successful restoration. Our method succeeds in reconstruction with even less time than the baseline, without the need for such excessive sampling. VR stands for variance reduction.

5 DISCUSSION

In this section, we provide two interpretations for the faster convergence of the proposed semi-gradient method, which eliminates the partial derivative for the RHS, compared to the baseline in Eq. (6). Additionally, we present an ablation study.

Bias. As demonstrated in Appendix B, the baseline is a biased estimator of the actual gradient of the loss. This bias arises from the correlation between $\nabla_{\theta}\langle R_{\theta}\rangle$ and $\langle R_{\theta}\rangle$ in the partial derivative with respect to the RHS. Such bias ultimately stems from the stochastic nature of $\langle R_{\theta}\rangle$. This bias in gradient estimation can impede the convergence to the minimum by SGD algorithm [Bottou 2010], as illustrated well by the results in Fig. 5, demonstrating the erroneous convergence due to bias.

Moreover, across various scenes depicted in Fig. 9, the results consistently appear darker than the reference when using the baseline method. This occurs because as scenes darken, the variance of $\langle R_{\theta}\rangle$ decreases, and so does the covariance between $\nabla_{\theta}\langle R_{\theta}\rangle$ and $\langle R_{\theta}\rangle$. Moreover, the expectation of the baseline gradient estimator is the sum of the actual gradient and the covariance between $\nabla_{\theta}\langle R_{\theta}\rangle$ and $\langle R_{\theta}\rangle$ (Eq. (25) in the Appendix). Therefore, the covariance must decrease for the expectation of the gradient estimator to become sufficiently small, causing the SGD algorithm to halt.

Similar issues regarding the stochasticity of MC estimates of rendering integrals causing bias in gradients have been noted in the field of inverse rendering [Azinovic et al. 2019; Nimier-David et al. 2020]. We extend this discussion to forward rendering as well.

On the contrary, while the semi-gradient loss shares the same minima as the baseline loss, its gradient estimator is not formulated as the product of $\nabla_{\theta}\langle R_{\theta}\rangle$ and $\langle R_{\theta}\rangle$, thus sidestepping the issue of bias.

Variance. However, bias is not the sole contributing factor. When employing the dual-buffer (or half-buffer) method [Deng et al. 2022; Pidhorskyi et al. 2022], which provides an unbiased estimator for the gradient of the L2 loss (see Appendix C), the overall brightness of the scene is well-reconstructed (see Fig. 5). Nonetheless, visual aspects such as glossy reflections do not achieve the highest quality of reconstruction within 36,000 iterations.

Therefore, we point to variance as another factor contributing to slow convergence. For both the baseline and dual-buffer methods, the RHS partial derivative involves the product of the two random variables, $\nabla_{\theta}\langle R_{\theta}\rangle$ and $\langle R_{\theta}\rangle$. Consequently, the overall variance corresponds to the product of the variances of these two variables, leading to excessive variance and hindering learning. In Fig. 5, increasing the incident sample count eightfold would reduce the variance in the RHS derivative, bringing the visual quality on par with ours and the reference. However, this requires 16 times more training time. Additionally, in the simple CornellBox scene at Fig. 7, the variance in RHS estimates would be certainly low, so the dual-buffer method converges as well as ours.

Meanwhile, the semi-gradient estimator, which entirely ignores the RHS derivative, is free from the burden of double variance.

Ablation study. In addition to theoretical results, to more clearly demonstrate the advantages of the semi-gradient estimator over an unbiased gradient estimator for the baseline loss (e.g., the dual-buffer method), we train neural caches by linearly combining the two gradient estimates. When the weight $w = 1$, the gradient estimator corresponds to the gradient estimator of the dual-buffer method, and when the $w = 0$, it corresponds to the semi-gradient estimator. Please refer to Appendix D for the implementation details of the weighted loss. In other words, by manipulating the weight associated with the RHS partial derivative, we can discern the impact on learning progression. Ultimately, Fig. 6 demonstrates that as RHS weights decrease, performance progressively improves, thus experimentally proving the detrimental effect of RHS partial derivatives on convergence.

6 LIMITATIONS AND FUTURE WORK

Our proposed method demonstrates numerical and visual improvements in most scenes (see Fig. 9), but there are certain scenes where the improvements are limited. As shown in the first row of Fig. 7, in simple scenes where the RHS can be accurately estimated through next event estimation, all models exhibit similar performance. Additionally, in the scenes shown in the second row, which can be easily rendered using simple path tracing, all models struggle to capture highly view-dependent reflection effects. The supplementary video of the TVRoom scene also shows similar difficulties in

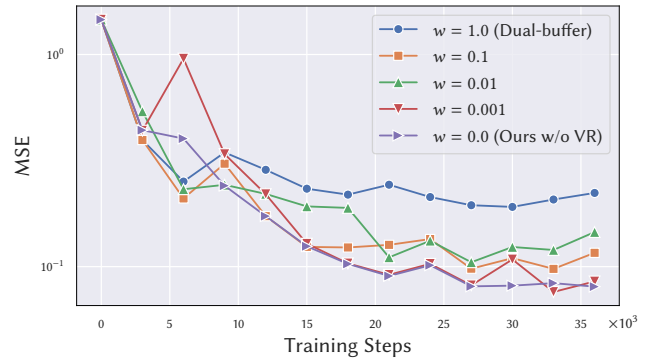


Fig. 6. Linear interpolation between the gradients of the dual-buffer and our method using weight w . The key difference between the two methods is whether the RHS partial derivative is included in the gradient. As the weight is reduced to 0, the influence of the RHS partial derivative diminishes, converging to the semi-gradient method, and the model’s performance improves. The figure displays the convergence of image error, averaged across seven scenes in Fig. 9. VR stands for variance reduction.

capturing reflections on rough glass surfaces on a TV. We aim to explore effective directional space learning techniques to overcome these challenges in future work.

Extending the semi-gradient technique to differentiable rendering is another intriguing problem. The challenges of physically-based differentiable rendering include 1) implementing and theorizing the derivative of the path integrals and 2) differentiation on noisy inputs, which hampers accurate gradient estimation. Recent studies have applied the advantages of residual training-based neural caches to differentiable rendering, excluding the need for path integral evaluation [Hadadan et al. 2023]. This allows derivatives of the path integral to be easily obtained using neural networks and automatic differentiation. Applying the semi-gradient technique here could avoid differentiation on noisy inputs, facilitating gradient estimation.

Additionally, applying the semi-gradient method to generic losses and extending the theory is an important future direction. Since the L2 loss is still widely used in many optimization-based global illumination (GI) fields [Balint et al. 2023; Deng et al. 2022; Fischer and Ritschel 2023; Nicolet et al. 2023; Pidhorskyi et al. 2022; Wang et al. 2023], the theoretical analysis of the semi-gradient method based on L2 is an important contribution to GI. Nevertheless, naively applying the semi-gradient method to generic losses is insufficient to address the bias in gradient estimation. This is because non-L2 losses do not enable unbiased derivative estimation in general [Nicolet et al. 2023]. Despite the limitation, our preliminary experiments (Fig. 8) show that the semi-gradient technique achieves 2-15 times lower image error compared to the baseline when using root mean square error (RMSE), Huber loss, and mean average error (MAE). These experimental results suggest that our fundamental intuition to ignore differentiation on the RHS, given its faster convergence compared to the LHS, remains valid and beneficial.

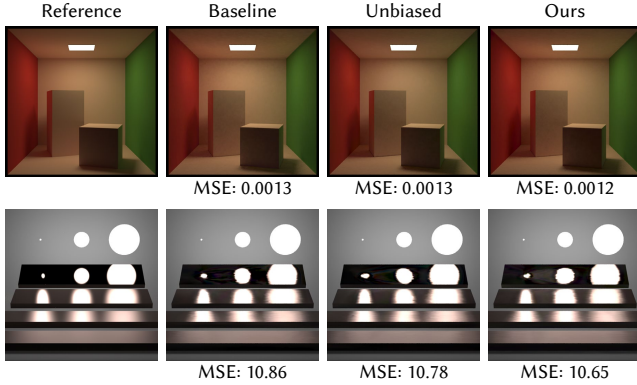


Fig. 7. Examples where our approach does not provide performance advantages. In the first row, where the scene is simple and the stochasticity of RHS estimates is low, the issues of bias and high variance in the baseline gradient estimator are already negligible. In the second row, as the plates become smoother, all models struggle with reconstruction. *Unbiased* refers to the model using the dual-buffer method.

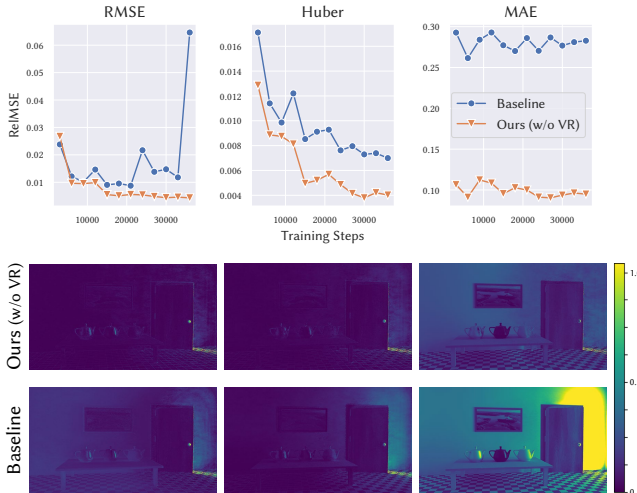


Fig. 8. Visualization of the convergence and final error maps when applying the semi-gradient and baseline techniques to optimize objective functions other than the L2 loss (e.g., RMSE, Huber, MAE). The semi-gradient method consistently reduces error more effectively than the baseline, even when using non-L2 objectives, which do not necessarily guarantee unbiased convergence. For better visualization, the RelMSE maps are tone-mapped, and the 0-th step errors are omitted in the first row.

7 CONCLUSION

This paper discusses an optimization technique based on partial derivatives to achieve faster and more accurate convergence in residual-based neural rendering methods. We start our discussion with the observation that the right-hand side (RHS), which is the sum of emitted and reflected radiance in the rendering integral, converges significantly faster than the left-hand side (LHS). By deviating from the traditional objective function that pulls the LHS and

RHS together, we employ a semi-gradient method that intentionally ignores updates to the RHS for neural cache training. This method achieves an average of 8.8 times lower image error across various scenes compared to existing methods, and reduces per-iteration time by 25-30% due to avoiding automatic differentiation on the RHS. Through several key proofs, we demonstrate that the semi-gradient loss achieves the same minimum as the existing baseline (i.e., the solution to the rendering equation), while being free from the bias and high variance issues that complicate accurate gradient estimation of the baseline loss. The empirical results show that this characteristic significantly improves training efficiency and rendering accuracy.

ACKNOWLEDGMENTS

The authors would like to thank the anonymous reviewers for their valuable comments and insightful suggestions. We also express our gratitude to Kyu Beom Han (KAIST) and our colleagues Jongho Park, Jaeseung Park, Jaeyoung Hwang, Taehong Moon, Byeong-Uk Lee, Minkyu Kim (KRAFTON) for their support and contributions. We also thank the following people for providing test scenes: Bitterli [2016], SlykDrako (Bed), Benedikt Bitterli (Bidir, Door), Marek (Bath), Wig42 (Greyroom)¹, NewSee2l035 (Hall)², and Jay-Artist (TVRoom)³. Special thanks to the KRAFTON’s KITCHEN 35 team for their invaluable nourishment during this project. Jaewoong Cho is the corresponding author of this paper.

¹<https://www.blendswap.com/blend/13552>

²<https://www.blendswap.com/blend/6304>

³<https://www.blendswap.com/blend/5014>

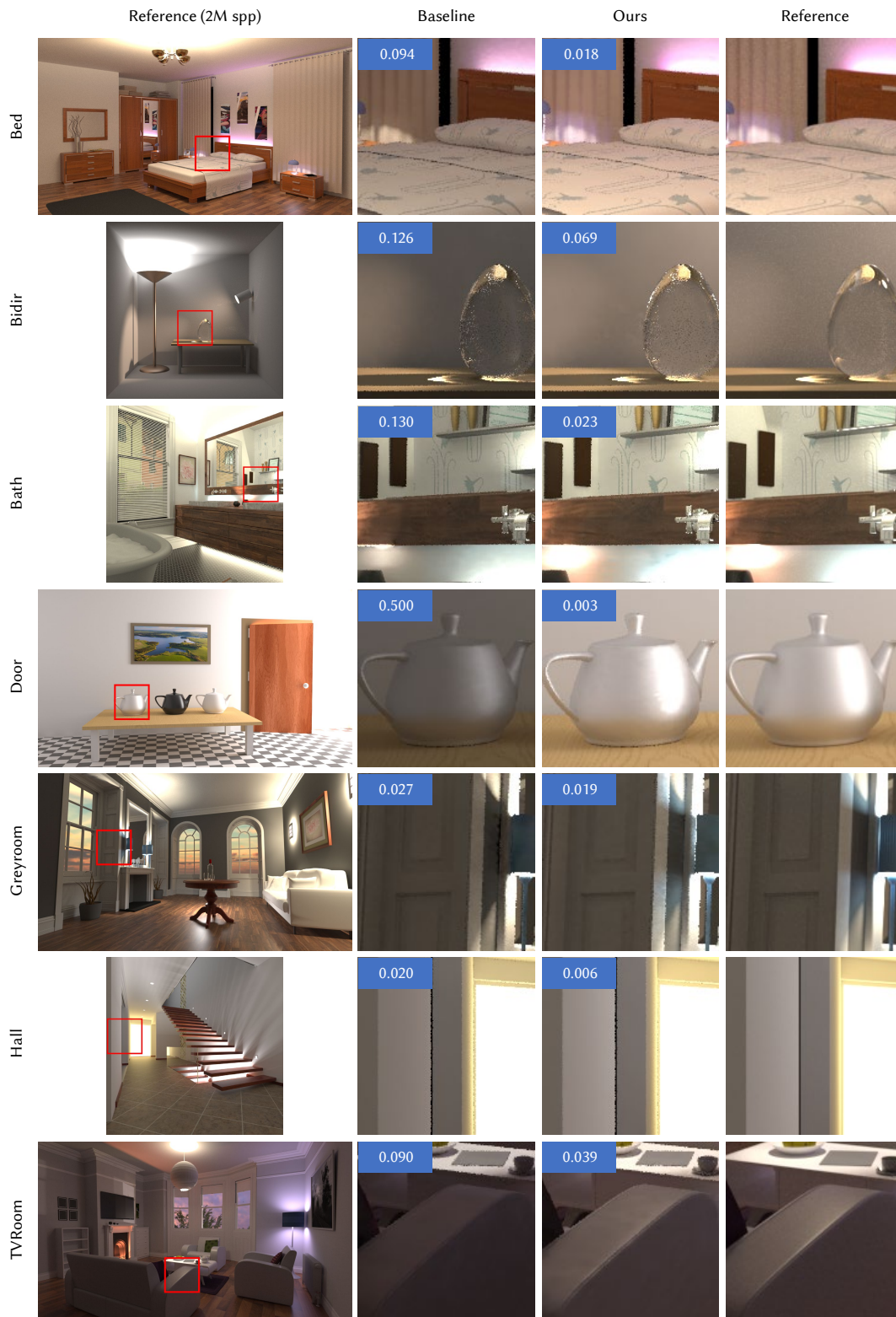


Fig. 9. Performance comparison after the same 36K training iterations. The RelMSE error displayed for each image indicates that our method results in a markedly lower whole-image distance toward the reference image. We recommend observing the visual improvements in details related to strong indirect light sources, caustics, reflections, and color bleeding.

REFERENCES

- Dejan Azinovic, Tzu-Mao Li, Anton Kaplanyan, and Matthias Nießner. 2019. Inverse path tracing for joint material and lighting estimation. In *Proceedings of the IEEE/CVF conference on computer vision and pattern recognition*. 2447–2456.
- Leemon Baird. 1995. Residual algorithms: Reinforcement learning with function approximation. In *Machine Learning Proceedings 1995*. Elsevier, 30–37.
- Martin Balint, Karol Myszkowski, Hans-Peter Seidel, and Gurprit Singh. 2023. Joint Sampling and Optimisation for Inverse Rendering. In *SIGGRAPH Asia 2023 Conference Papers*. 1–10.
- Benedikt Bitterli. 2016. Rendering resources. <https://benedikt-bitterli.me/resources/>
- Léon Bottou. 2010. Large-scale machine learning with stochastic gradient descent. In *Proceedings of COMPSTAT 2010: 19th International Conference on Computational Statistics Paris France, August 22-27, 2010 Keynote, Invited and Contributed Papers*. Springer, 177–186.
- In-Young Cho. 2023. *Implementation Tutorial for Neural Radiosity [Hadadan et al. 2021]*. Accessed: 2023-05-30.
- Arno Coomans, Edoardo A Dominci, Christian Döring, Joerg H Mueller, Jozef Hladky, and Markus Steinberger. 2024. Real-time Neural Rendering of Dynamic Light Fields. In *Computer Graphics Forum*. Wiley Online Library, e15014.
- Xi Deng, Fujun Luan, Bruce Walter, Kavita Bala, and Steve Marschner. 2022. Reconstructing translucent objects using differentiable rendering. In *ACM SIGGRAPH 2022 Conference Proceedings*. 1–10.
- Honghao Dong, Guoping Wang, and Sheng Li. 2023. Neural Parametric Mixtures for Path Guiding. In *ACM SIGGRAPH 2023 Conference Proceedings*. ACM, 1–10.
- Michael Fischer and Tobias Ritschel. 2023. Plateau-reduced differentiable path tracing. In *Proceedings of the IEEE/CVF Conference on Computer Vision and Pattern Recognition*. 4285–4294.
- Xavier Glorot and Yoshua Bengio. 2010. Understanding the difficulty of training deep feedforward neural networks. In *Proceedings of the thirteenth international conference on artificial intelligence and statistics*. JMLR Workshop and Conference Proceedings, 249–256.
- Saeed Hadadan, Shuhong Chen, and Matthias Zwicker. 2021. Neural radiosity. *ACM Transactions on Graphics (TOG)* 40, 6 (2021), 1–11.
- Saeed Hadadan, Geng Lin, Jan Novák, Fabrice Rousselle, and Matthias Zwicker. 2023. Inverse Global Illumination using a Neural Radiometric Prior. In *ACM SIGGRAPH 2023 Conference Proceedings*. ACM, 1–11.
- Jiawei Huang, Akito Iizuka, Hajime Tanaka, Taku Komura, and Yoshifumi Kitamura. 2024. Online Neural Path Guiding with Normalized Anisotropic Spherical Gaussians. *ACM Transactions on Graphics* 43, 3 (2024), 1–18.
- Wenzel Jakob, Sébastien Speierer, Nicolas Roussel, Merlin Nimier-David, Delio Vicini, Tizian Zeltner, Baptiste Nicolet, Miguel Crespo, Vincent Leroy, and Ziyi Zhang. 2022. *Mitsuba 3 renderer*. <https://mitsuba-renderer.org>.
- James T. Kajiya. 1986. The Rendering Equation. In *Proceedings of the 13th Annual Conference on Computer Graphics and Interactive Techniques (SIGGRAPH '86)*. Association for Computing Machinery, New York, NY, USA, 143–150. <https://doi.org/10.1145/15922.15902>
- Diederik P Kingma and Jimmy Ba. 2014. Adam: A method for stochastic optimization. *arXiv preprint arXiv:1412.6980* (2014).
- Mingrui Liu, Wei Zhang, Francesco Orabona, and Tianbao Yang. 2020. Adam⁺: A Stochastic Method with Adaptive Variance Reduction. *arXiv preprint arXiv:2011.11985* (2020).
- Volodymyr Mnih, Koray Kavukcuoglu, David Silver, Andrei A Rusu, Joel Veness, Marc G Bellemare, Alex Graves, Martin Riedmiller, Andreas K Fiedelnd, Georg Ostrovski, et al. 2015. Human-level control through deep reinforcement learning. *nature* 518, 7540 (2015), 529–533.
- Thomas Müller. 2021. *tiny-cuda-nn*. <https://github.com/NVlabs/tiny-cuda-nn>
- Thomas Müller, Alex Evans, Christoph Schied, and Alexander Keller. 2022. Instant Neural Graphics Primitives with a Multiresolution Hash Encoding. *ACM Trans. Graph.* 41, 4, Article 102 (July 2022), 15 pages. <https://doi.org/10.1145/3528223.3530127>
- Thomas Müller, Fabrice Rousselle, Jan Novák, and Alexander Keller. 2021. Real-time neural radiance caching for path tracing. *ACM Transactions on Graphics (TOG)* 40, 4 (2021), 1–16.
- Laszlo Neumann and Attila Neumann. 1995. Radiosity and hybrid methods. *ACM Transactions on Graphics (TOG)* 14, 3 (1995), 233–265.
- Baptiste Nicolet, Fabrice Rousselle, Jan Novak, Alexander Keller, Wenzel Jakob, and Thomas Müller. 2023. Recursive Control Variates for Inverse Rendering. *ACM Transactions on Graphics (TOG)* 42, 4 (2023), 1–13.
- Merlin Nimier-David, Sébastien Speierer, Benoit Ruiz, and Wenzel Jakob. 2020. Radiative backpropagation: An adjoint method for lightning-fast differentiable rendering. *ACM Transactions on Graphics (TOG)* 39, 4 (2020), 146–1.
- Steven G Parker, James Bigler, Andreas Dietrich, Heiko Friedrich, Jared Hoberock, David Luebke, David McAllister, Morgan McGuire, Keith Morley, Austin Robison, et al. 2010. Optix: a general purpose ray tracing engine. *Acm transactions on graphics (tog)* 29, 4 (2010), 1–13.
- Adam Paszke, Sam Gross, Soumith Chintala, Gregory Chanan, Edward Yang, Zachary DeVito, Zeming Lin, Alban Desmaison, Luca Antiga, and Adam Lerer. 2017. Automatic differentiation in pytorch. (2017).
- Stanislav Pidhorskyi, Timur Bagautdinov, Shugao Ma, Jason Saragih, Gabriel Schwartz, Yaser Sheikh, and Tomas Simon. 2022. Depth of Field Aware Differentiable Rendering. *ACM Transactions on Graphics (TOG)* 41, 6 (2022), 1–18.
- Gilles Rainer, Adrien Bousseau, Tobias Ritschel, and George Drettakis. 2022. Neural precomputed radiance transfer. In *Computer Graphics Forum*, Vol. 41. Wiley Online Library, 365–378.
- Adam Scibior and Frank Wood. 2021. Differentiable particle filtering without modifying the forward pass. *arXiv preprint arXiv:2106.10314* (2021).
- Arsalan Sharifnassab and Richard S Sutton. 2023. Toward efficient gradient-based value estimation. In *International Conference on Machine Learning*. PMLR, 30827–30849.
- Delio Vicini, Sébastien Speierer, and Wenzel Jakob. 2021. Path replay backpropagation: differentiating light paths using constant memory and linear time. *ACM Transactions on Graphics (TOG)* 40, 4 (2021), 1–14.
- Chong Wang, Xi Chen, Alexander J Smola, and Eric P Xing. 2013. Variance reduction for stochastic gradient optimization. *Advances in neural information processing systems* 26 (2013).
- Yu-Chen Wang, Chris Wyman, Lifan Wu, and Shuang Zhao. 2023. Amortizing Samples in Physics-Based Inverse Rendering Using ReSTIR. *ACM Transactions on Graphics (TOG)* 42, 6 (2023), 1–17.
- Shuyu Yin, Tao Luo, Peilin Liu, and Zhi-Qin John Xu. 2022. An Experimental Comparison Between Temporal Difference and Residual Gradient with Neural Network Approximation. *arXiv preprint arXiv:2205.12770* (2022).
- Cheng Zhang, Zhao Dong, Michael Doggett, and Shuang Zhao. 2021. Antithetic sampling for Monte Carlo differentiable rendering. *ACM Transactions on Graphics (TOG)* 40, 4 (2021), 1–12.
- Shangtong Zhang, Wendelin Boehmer, and Shimon Whiteson. 2019. Deep residual reinforcement learning. *arXiv preprint arXiv:1905.01072* (2019).
- Junqiu Zhu, Yaoyi Bai, Zilin Xu, Steve Bako, Edgar Velázquez-Armendáriz, Lu Wang, Pradeep Sen, Milos Hasan, and Ling-Qi Yan. 2021. Neural complex luminaires: representation and rendering. *ACM Transactions on Graphics (TOG)* 40, 4 (2021), 57–1.

A CONVERGENCE OF GRADIENT DESCENT FOR THE SEMI-GRADIENT LOSS

We first reformulate the rendering equation (Eq. (1) of the main report) using the light transport operator T for a concise derivation:

$$L^* = E + T \circ L^*, \quad (9)$$

where T takes an outgoing radiance field, proceeds ray tracing, integrals scattering events, and outputs a reflected radiance field.

For a physically correct scene, T is a contraction mapping satisfying:

$$\exists \lambda \in (0, 1) : \forall L, \|T \circ L\| \leq \lambda \|L\|. \quad (10)$$

That is, roughly speaking, for an arbitrary radiance field L , the energy of the reflected radiance field reduces from that of L (i.e., energy absorption) [Neumann and Neumann 1995].

Then, we can also reformulate the semi-gradient loss using T :

$$\mathcal{L}_{SG}(L) = \|L - \text{sg}(E + T \circ L)\|^2, \quad (11)$$

where we denote the stop-gradient operator as $\text{sg}(\cdot)$ and omit the normalization.

Taking the gradient with respect to L , we have:

$$\nabla_L \mathcal{L}_{SG}(L) = 2(L - E - \text{sg}(T \circ L)) \quad (12)$$

$$= 2(L - E - T \circ L) \quad (\text{in evaluation}) \quad (13)$$

Consider gradient descent with learning rate $\alpha_{k \geq 1} > 0$ for any initial radiance field L_0 . The update rule for $k \geq 1$ is:

$$L_k = L_{k-1} - \alpha_k \nabla \mathcal{L}_{SG}(L_{k-1}) \quad (14)$$

Setting $\alpha_k = \frac{1}{2}$ for all k , we can show that the gradient descent converges to L^* for any L_0 .

The key insight is that T is a contraction mapping. This guarantees that repeated applications of T shrink the error towards zero. Mathematically, we have:

$$\|L_k - L^*\| = \left\| \left(L_{k-1} - \frac{1}{2} \nabla \mathcal{L}_{\text{SG}}(L_{k-1}) \right) - (E + T \circ L^*) \right\| \quad (15)$$

$$= \|L_{k-1} - L_{k-1} + E + T \circ L_{k-1} - E - T \circ L^*\| \quad (16)$$

$$= \|T \circ (L_{k-1} - L^*)\| \quad (17)$$

$$= \|T^k \circ (L_0 - L^*)\|. \quad (18)$$

By the contraction mapping property:

$$\|L_k - L^*\| = \|T^k \circ (L_0 - L^*)\| \quad (19)$$

$$= \|T \circ T^{k-1} \circ (L_0 - L^*)\| \quad (20)$$

$$\leq \lambda \|T^{k-1} \circ (L_0 - L^*)\| \quad (21)$$

Continuing in a recursive manner, we get:

$$\leq \lambda^k \|L_0 - L^*\| \quad (22)$$

Therefore, as k approaches infinity, the error $\|L_k - L^*\|$ goes to zero, implying convergence to L^* :

$$\lim_{k \rightarrow \infty} \|L_k - L^*\| = 0 \quad (23)$$

Consequently, we find a sequence of gradient descent along $\nabla \mathcal{L}_{\text{SG}}$ that converges to L^* , which is the solution of the rendering equation, regardless of the starting point L_0 . ■

B BIASEDNESS OF THE BASELINE GRADIENT ESTIMATOR

To prove the biasedness of the baseline gradient estimator, we need to show that the expectation of the gradient estimator $\mathbb{E}[\nabla_\theta \langle \mathcal{L}(\theta) \rangle_{\text{NR}}]$ is *not equal* to the true gradient $\nabla_\theta \mathcal{L}(\theta)$ at some (x, ω) and θ . Let us first derive the true gradient as follows:

$$\nabla_\theta \mathcal{L}(\theta) = \nabla_\theta L_\theta \cdot \frac{2(L_\theta - R_\theta)}{\|L_\theta\|^2 + \epsilon} + \nabla_\theta R_\theta \cdot \frac{-2(L_\theta - R_\theta)}{\|L_\theta\|^2 + \epsilon}. \quad (24)$$

Also, by Eq. (6) of the main report, the expectation of the baseline gradient estimator is:

$$\begin{aligned} \mathbb{E}[\nabla_\theta \langle \mathcal{L}(\theta) \rangle_{\text{NR}}] &= \nabla_\theta L_\theta \cdot \frac{2(L_\theta - \mathbb{E}[\langle R_\theta \rangle])}{\|L_\theta\|^2 + \epsilon} \\ &\quad + \frac{-2(\mathbb{E}[\nabla_\theta \langle R_\theta \rangle] \cdot L_\theta - \mathbb{E}[\nabla_\theta \langle R_\theta \rangle \cdot \langle R_\theta \rangle])}{\|L_\theta\|^2 + \epsilon}, \\ &= \nabla_\theta L_\theta \cdot \frac{2(L_\theta - R_\theta)}{\|L_\theta\|^2 + \epsilon} \\ &\quad + \frac{-2(\nabla_\theta R_\theta \cdot L_\theta - \mathbb{E}[\nabla_\theta \langle R_\theta \rangle \cdot \langle R_\theta \rangle])}{\|L_\theta\|^2 + \epsilon}. \end{aligned} \quad (25)$$

Considering the difference between the above two equations, it suffices to show that the inequality $\nabla_\theta R_\theta \cdot R_\theta \neq \mathbb{E}[\nabla_\theta \langle R_\theta \rangle \cdot \langle R_\theta \rangle]$ for proving the biasedness (i.e., $\nabla_\theta \mathcal{L}(\theta) \neq \mathbb{E}[\nabla_\theta \langle \mathcal{L}(\theta) \rangle_{\text{NR}}]$).

Let us start by proving that $\nabla_\theta R_\theta \cdot R_\theta = \mathbb{E}[\nabla_\theta \langle R_\theta \rangle \cdot \langle R_\theta \rangle]$ if and only if the variance of the RHS estimate is constant (for every θ). Then, we will claim that the variance of the RHS estimate cannot

be constant, which negates the equality, proving the biasedness of the gradient estimator.

Suppose that the variance of the RHS estimate is constant for θ . That is, there exists a constant $c \in \mathbb{R}$, such that $\text{Var}[\langle R_\theta \rangle] = c$ at every θ . Therefore,

$$\begin{aligned} \nabla_\theta (\text{Var}[\langle R_\theta \rangle]) &= 0, \\ \nabla_\theta (\mathbb{E}[\langle R_\theta \rangle^2] - \mathbb{E}[\langle R_\theta \rangle]^2) &= 0. \end{aligned} \quad (26)$$

By the Leibniz integral rule, we can interchange the differentials and expectations (i.e., integrals) in the last equation:

$$\begin{aligned} \mathbb{E}[2\nabla_\theta \langle R_\theta \rangle \cdot \langle R_\theta \rangle] - 2\nabla_\theta (\mathbb{E}[\langle R_\theta \rangle]) \cdot \mathbb{E}[\langle R_\theta \rangle] &= 0, \\ \mathbb{E}[2\nabla_\theta \langle R_\theta \rangle \cdot \langle R_\theta \rangle] - 2\nabla_\theta R_\theta \cdot R_\theta &= 0. \end{aligned} \quad (27)$$

Thus we proved the one direction.

The converse is also true. If $\nabla_\theta (\text{Var}[\langle R_\theta \rangle]) = 0$ for every θ , then there does not exist two parameters, θ_1 and θ_2 , such that $\text{Var}[\langle R_{\theta_1} \rangle] \neq \text{Var}[\langle R_{\theta_2} \rangle]$ by the mean value theorem. It proves that the variance is constant for θ if $\nabla_\theta R_\theta \cdot R_\theta = \mathbb{E}[\nabla_\theta \langle R_\theta \rangle \cdot \langle R_\theta \rangle]$.

The variance of the RHS estimate indeed is not constant for θ . Since the variance can be zero when our radiance prediction network produces zeros at all inputs (e.g., $\theta = 0$), and the variance can evidently be positive with some θ s (e.g., Fig. 5 of the main report).

Therefore, the inequality $\nabla_\theta \mathcal{L}(\theta) \neq \mathbb{E}[\nabla_\theta \langle \mathcal{L}(\theta) \rangle_{\text{NR}}]$ holds, which means the gradient of the baseline estimator is biased to the true gradient of the baseline loss. ■

C UNBIASEDNESS OF THE DUAL-BUFFER GRADIENT ESTIMATOR

To prove the unbiasedness of the dual-buffer gradient estimator, we need to show that the expectation of the gradient estimator $\mathbb{E}[\nabla_\theta \langle \mathcal{L}(\theta) \rangle_{\text{DB}}]$ is *equal* to the true gradient $\nabla_\theta \mathcal{L}(\theta)$ at every (x, ω) and θ .

First, the dual-buffer loss estimator is:

$$\langle \mathcal{L}(\theta) \rangle_{\text{DB}} = \frac{(L_\theta - \langle R_\theta \rangle_X) \cdot (L_\theta - \langle R_\theta \rangle_Y)}{\|\text{sg}(L_\theta)\|^2 + \epsilon}, \quad (28)$$

where $\langle R_\theta \rangle_X$ and $\langle R_\theta \rangle_Y$ are two uncorrelated estimates of R_θ .

Then, the expectation of the gradient of the dual-buffer estimator is:

$$\begin{aligned} \mathbb{E}[\nabla_\theta \langle \mathcal{L}(\theta) \rangle_{\text{DB}}] &= \mathbb{E} \left[\nabla_\theta \left(\frac{\|L_\theta\|^2 - L_\theta \cdot (\langle R_\theta \rangle_X + \langle R_\theta \rangle_Y)}{\|\text{sg}(L_\theta)\|^2 + \epsilon} \right) \right] \\ &\quad + \mathbb{E} \left[\nabla_\theta \left(\frac{\langle R_\theta \rangle_X \cdot \langle R_\theta \rangle_Y}{\|\text{sg}(L_\theta)\|^2 + \epsilon} \right) \right], \\ &= \nabla_\theta \left(\frac{\|L_\theta\|^2 - L_\theta \cdot (\mathbb{E}[\langle R_\theta \rangle_X] + \mathbb{E}[\langle R_\theta \rangle_Y])}{\|\text{sg}(L_\theta)\|^2 + \epsilon} \right) \\ &\quad + \nabla_\theta \left(\frac{\mathbb{E}[\langle R_\theta \rangle_X \cdot \langle R_\theta \rangle_Y]}{\|\text{sg}(L_\theta)\|^2 + \epsilon} \right), \\ &= \nabla_\theta \left(\frac{\|L_\theta\|^2 - 2L_\theta \cdot R_\theta}{\|\text{sg}(L_\theta)\|^2 + \epsilon} \right) \\ &\quad + \nabla_\theta \left(\frac{\mathbb{E}[\langle R_\theta \rangle_X] \cdot \mathbb{E}[\langle R_\theta \rangle_Y]}{\|\text{sg}(L_\theta)\|^2 + \epsilon} \right). \end{aligned} \quad (29)$$

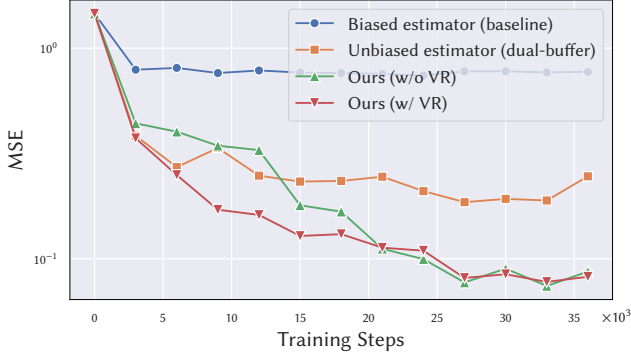


Fig. 10. Ablation study on our models with and without an additional path guiding module for variance reduction on the RHS and gradient estimator. We also visualize the dual-buffer method for the reference.

By the Leibniz integral rule, we can interchange the differentials and expectations (i.e., integrals) in the above equations.

The last equality holds since two estimates, $\langle R_\theta \rangle_X$ and $\langle R_\theta \rangle_Y$, are supposed to be uncorrelated in the dual-buffer method. Therefore, starting from the last equality,

$$\begin{aligned}
 \mathbb{E}[\nabla_\theta \langle \mathcal{L}_{\text{DB}}(\theta) \rangle] &= \nabla_\theta \left(\frac{\|L_\theta\|^2 - 2L_\theta \cdot R_\theta}{\|\text{sg}(L_\theta)\|^2 + \epsilon} \right) + \nabla_\theta \left(\frac{R_\theta \cdot R_\theta}{\|\text{sg}(L_\theta)\|^2 + \epsilon} \right), \\
 &= \frac{\nabla_\theta L_\theta \cdot (2L_\theta - 2R_\theta) + \nabla_\theta R_\theta \cdot (-2L_\theta)}{\|L_\theta\|^2 + \epsilon} \\
 &\quad + \frac{2\nabla_\theta R_\theta \cdot R_\theta}{\|L_\theta\|^2 + \epsilon}, \\
 &= \nabla_\theta \mathcal{L}(\theta),
 \end{aligned} \tag{30}$$

which shows that the gradient of the dual-buffer estimator is unbiased to the true gradient of the baseline loss. ■

D WEIGHTED DUAL-BUFFER METHOD FOR ABLATION

To investigate how the partial derivative with respect to the RHS of Eq. (28) affects the reconstruction quality, we define the following weighted dual-buffer estimator given a non-negative scalar weight w :

$$\begin{aligned}
 \langle \mathcal{L}(\theta; w) \rangle_{\text{WDB}} &= \frac{\left\| L_\theta - \text{sg} \left(\frac{\langle R_\theta \rangle_X + \langle R_\theta \rangle_Y}{2} \right) \right\|^2}{\|\text{sg}(L_\theta)\|^2 + \epsilon} \\
 &\quad + w \cdot \frac{(\text{sg}(L_\theta) - \langle R_\theta \rangle_X) \cdot (\text{sg}(L_\theta) - \langle R_\theta \rangle_Y)}{\|\text{sg}(L_\theta)\|^2 + \epsilon},
 \end{aligned} \tag{31}$$

where $\langle R_\theta \rangle_X$ and $\langle R_\theta \rangle_Y$ are two uncorrelated estimates of R_θ . The gradient of the weighted dual-buffer estimator is derived as follows:

$$\begin{aligned}
 \nabla_\theta \langle \mathcal{L}(\theta; w) \rangle_{\text{WDB}} &= \nabla_\theta L_\theta \cdot \frac{2L_\theta - (\langle R_\theta \rangle_X + \langle R_\theta \rangle_Y)}{\|L_\theta\|^2 + \epsilon} \\
 &\quad + w \cdot \nabla_\theta \langle R_\theta \rangle_X \cdot \frac{-(L_\theta - \langle R_\theta \rangle_Y)}{\|L_\theta\|^2 + \epsilon} \\
 &\quad + w \cdot \nabla_\theta \langle R_\theta \rangle_Y \cdot \frac{-(L_\theta - \langle R_\theta \rangle_X)}{\|L_\theta\|^2 + \epsilon}.
 \end{aligned} \tag{32}$$

Therefore, it can modulate the influence of the RHS derivatives on network parameter updates by varying the weight w . We thus refer to it as a *weighted* dual-buffer estimator. At $w = 1$, the gradient of the weighted dual-buffer estimator is equivalent to the gradient of the vanilla dual-buffer estimator, and setting $w = 0$ induces the gradient of the semi-gradient estimator.